

Temperature from quantum entanglement

S. Santhosh Kumar* and S. Shankaranarayanan†

School of Physics, Indian Institute of Science Education and Research(IISER-TVM), Thiruvananthapuram- 695 016, India

It is still unclear how thermal states dynamically emerge from a microscopic quantum description. A complete understanding of the long time evolution of closed quantum systems may resolve the tension between a microscopic description and the one offered by equilibrium statistical mechanics. In an attempt in this direction, we consider a simple bipartite system (a quantum scalar field propagating in black-hole background) and study the evolution of the entanglement entropy — by tracing over the degrees of freedom inside the event-horizon — at different times. We define *entanglement temperature* which is similar to the one used in the microcanonical ensemble picture in statistical mechanics and show that (i) this temperature is a finite quantity while the entanglement entropy diverges and (ii) matches with the Hawking temperature for all several black-hole spacetimes. We also discuss the implications of our result for the laws of black-hole mechanics and eigen-state thermalization.

PACS numbers: 03.67.Mn, 05.50.+q, 05.70.-a, 04.70.Dy

INTRODUCTION

Equilibrium statistical mechanics, as pioneered by Boltzmann and Gibbs, provides a relation between the density operator of a system under various external conditions and the emergent properties of the matter in terms of the thermodynamical quantities. More specifically, equilibrium statistical mechanics is governed by the phase space distribution whose knowledge enables one to find various (close to) equilibrium properties of a system [1]

In the same spirit, over the last three decades, the key question that has been asked in different areas of physics is: *What is the relationship between the quantum entanglement and the emergent properties of the matter?* [2–4]. For instance: (i) The fundamental law of quantum information processing states that entanglement cannot be increased by local operations [5, 6]. This law is identical to the second law that says that thermodynamical entropy cannot decrease in an isolated system. One hopes that thermodynamics may help in understanding quantum theory [7]. (ii) In the case of quantum phase transitions, the interactions induce quantum entanglement. Also, the same interactions play a significant role in determining the emergent properties of the system. There are many attempts to find the relationship between quantum entanglement and quantum phase transition [8–10]. (iii) In the case of gravity, it is emerging that the physics across event horizons plays an important role and the first connections were seen by Bekenstein [11–13]. Jacobson [14] showed that the thermal properties across such horizons reproduce the entire structure of Einstein’s equations. Since then a number of proposals have been made along the lines of emergent gravity [15, 16]. (see also Ref. [17].)

However, our understanding of quantum entanglement is still very limited. In fact, quantum entanglement can be unambiguously quantified only for bipartite sys-

tems [18, 19]. While the bipartite system is an approximation for applications to condensed matter systems, however, in the case of black-holes, the event horizon provides a natural boundary. Besides, quantum entanglement and black-hole entropy/temperature are both purely quantum effects. Over the last three decades, there has been a large body of literature to associate the microscopic origin of black-hole entropy due to quantum entanglement of modes across the horizon [20–26].

However, entanglement as a source of black-hole entropy has a couple of drawbacks: (i) The proportionality constant depends on the ultra-violet cut-off and the number of fields present. Recently, it was shown that due to new scaling symmetries of the entanglement, the ultra-violet divergence can be mapped to an IR divergence [27] and (ii) It is not clear whether the entanglement entropy lead to the laws of black-hole mechanics. More specifically, whether one can recover Hawking temperature from the quantum entanglement of modes across the horizon.

In this work, we explicitly show that the *microcanonical temperature* obtained from entanglement entropy is identical to the Hawking temperature and satisfies the first law of black-hole mechanics. To evaluate entanglement entropy of the massless scalar field propagating in $(D + 2)$ -dimensional spherically symmetric space-time, we use the *direct approach* — discretize the Hamiltonian and evaluate the reduced density matrix in the real space — instead of the conformal field theory techniques [28]. The principal reason is that, as shown recently [27], entanglement entropy may have more symmetries than the classical Lagrangian/Hamiltonian of the system.

To remove the spurious effects due to the coordinate singularity at the horizon¹, we consider Lemaître coordi-

¹ In Refs.[29, 30], in the Schwarzschild coordinate, one need to bipartite the region $r > 2M$.

nate which is explicitly time-dependent[31]. One of the features that we exploit in our computation is the following: For a fixed Lemaître time coordinate, Hamiltonian of the scalar field in Schwarzschild space-time reduces to the scalar field Hamiltonian in flat space-time [32]. We perturbatively evolve the Hamiltonian about the fixed Lemaître time and obtain the entanglement entropy at different times. We show that all times, the entanglement entropy satisfies the area law, however, the value of the entropy is different at different times. We explicitly show that ratio of the change in the energy to the change in the entropy is identical to the Hawking temperature for 4- and 6-dimensional Schwarzschild, Reissner-Nordström and 6-dimensional Boulware-Deser[33].

Throughout this work, the metric signature we adopt is $(+, -, -, \dots)$ and set $\hbar = k_B = c = 1$, and $G = 1$.

SCALAR FIELD HAMILTONIAN IN LEMAÎTRE COORDINATES

Th action for the massless, real scalar field $\Phi(x^\mu)$ propagating in $(D + 2)$ -dimensional space-time is

$$S = \frac{1}{2} \int d^{D+2} \mathbf{x} \sqrt{-g} g^{\mu\nu} \partial_\mu \Phi(\mathbf{x}) \partial_\nu \Phi(\mathbf{x}) \quad (1)$$

where $g_{\mu\nu}$ is the Lemaître metric and is given by

$$ds^2 = d\tau^2 - (1 - f[r(\tau, \xi)]) d\xi^2 - r^2(\tau, \xi) d\Omega_D^2 \quad (2)$$

where τ, ξ are the time and radial components in Lemaître coordinates, respectively, r is the radial distance in Schwarzschild coordinate and $d\Omega_D$ is the D -dimensional angular line-element. τ and ξ are related by [31]

$$\xi - \tau = \int \frac{dr}{\sqrt{1 - f[r(\tau, \xi)]}} \quad (3)$$

In order for the line-element (2) to describe a black hole, the space-time must contain a singularity (say at $r = 0$) and have horizons. In this work, we assume that the space-time contains one non-degenerate event-horizon at r_h and that it is asymptotically flat. The specific form of $f(r)$ corresponds to different space-time.

The symmetry of the Lemaître metric (2) allows us to decompose the normal modes of the scalar field as: $\Phi(\mathbf{x}) = \sum_{l, m_i} \Phi_{lm_i}(\tau, \xi) Z_{lm_i}(\theta, \phi_i)$, where $i \in \{1, 2, \dots, D-1\}$ and Z_{lm_i} are the real hyper-spherical harmonics. We define the following dimensionless parameters: $\tilde{r} = r/r_h$, $\tilde{\xi} = \xi/r_h$, $\tilde{\tau} = \tau/r_h$, $\tilde{\Phi}_{lm_i} = r_h \Phi_{lm_i}$. Substituting Eq. (2) in the action (1) and using the orthogonal properties of Z_{lm_i} , we get,

$$S = \frac{1}{2} \sum_{l, m_i} \int d\tilde{\tau} d\tilde{\xi} \tilde{r}^D \left[\sqrt{1 - f[\tilde{r}]} (\partial_{\tilde{\tau}} \tilde{\Phi}_{lm_i})^2 - \frac{(\partial_{\tilde{\xi}} \tilde{\Phi}_{lm_i})^2}{\sqrt{1 - f[\tilde{r}]}} - \sqrt{1 - f[\tilde{r}]} \frac{l(l + D - 1)}{\tilde{r}^2} \tilde{\Phi}_{lm_i}^2 \right] \quad (4)$$

Noting that the line-element (2) is explicitly time-dependent and that the radial coordinate ξ is related to τ via relation (3), we expand the action in Eq.(4) via infinitesimal transformation of ξ and τ [34]:

$$\tilde{\tau} \rightarrow \tilde{\tau}' = \tilde{\tau} + \epsilon, \quad \tilde{\xi} \rightarrow \tilde{\xi}' = \tilde{\xi}, \quad (5a)$$

$$\tilde{\Phi}_{lm_i}(\tilde{\tau}, \tilde{\xi}) \rightarrow \tilde{\Phi}'_{lm_i}(\tilde{\tau}', \tilde{\xi}') = \tilde{\Phi}_{lm_i}(\tilde{\tau}, \tilde{\xi}), \quad (5b)$$

$$\tilde{r}(\tilde{\tau}', \tilde{\xi}') = \tilde{r}(\tilde{\tau} + \epsilon, \tilde{\xi}) \quad (5c)$$

Defining canonical conjugate momenta, we obtain Hamiltonian upto second order as

$$H \simeq H_0 + \epsilon V_1 + \epsilon^2 V_2 \quad (6)$$

where H_0 , V_1 and V_2 are defined in Appendix (A)(Appendix A contains detailed calculations).

The above Hamiltonian is key equation regarding which we would like to stress the following points: First, in the limit of $\epsilon \rightarrow 0$, the Hamiltonian reduces to that of a free scalar field propagating in flat space-time [32]. In other words, the zeroth order Hamiltonian is identical for all the space-times. Higher order ϵ terms contain information about the global space-time structure and, more importantly, the horizon properties. Second, the Lemaître coordinate is intrinsically time-dependent; the ϵ expansion of the Hamiltonian corresponds to the perturbation about the Lemaître time. Evaluation of the entanglement entropy (EE) for different values of ϵ corresponds to different values of Lemaître time. Third, it is not possible to obtain a closed form analytic expression for the density matrix (tracing out the quantum degrees of freedom associated with the scalar field inside a spherical region of radius r_h) and hence, we need to resort to numerical methods. In order to do that we take a spatially uniform radial grid, $\{\tilde{r}_j\}$, with $a = \tilde{r}_{j+1} - \tilde{r}_j$. We discretize the Hamiltonian (23) for different space-times.

The procedure to obtain the entanglement entropy for different ϵ is similar to the one discussed in Refs. [21, 24]. In this work we assume that the quantum state corresponding to the discretized Hamiltonian (23) is the ground state with wave-function $\Psi_{GS}(x_1, \dots, x_n; y_1, \dots, y_{N-n})$. The reduced density matrix $\rho(\vec{y}, \vec{y}')$ is obtained by tracing over the first n of the N oscillators $\int (\prod_{i=1}^n dx_i) \Psi_{GS}^*(x_1, \dots, x_n; \vec{y}) \Psi_{GS}(x_1, \dots, x_n; \vec{y}')$. In this work, we use Rényi entropy

$$S_\alpha = \frac{1}{1 - \alpha} \ln(\text{Tr} \rho^\alpha) \quad (7)$$

to be the measure of entanglement. In the limit of $\alpha \rightarrow 1$, S_α reduces to von Neumann entropy. Also, Rényi entropy provides a convergent alternative to the measure of entanglement for all space-time dimensions [26]. For $D = 2$, we obtain entanglement entropy for $\alpha = 1$, while for higher dimensions we obtain for different values of α .

Fourth, in analogy with microcanonical ensemble picture of equilibrium statistical mechanics, evaluation of

the Hamiltonian (23) at different ϵ , corresponds to setting the system at different internal energies. In analogy we define *entanglement temperature* [35]:

$$\frac{1}{T_{EE}} = \frac{1}{\alpha} \frac{\Delta S_\alpha}{\Delta E} = \frac{1}{\alpha} \frac{\text{Slope of EE}(\Delta S_\alpha/\Delta\epsilon)}{\text{Slope of energy}(\Delta E/\Delta\epsilon)} \quad (8)$$

In other words, we calculate the change in the ground state energy (entanglement entropy) for different values of ϵ and find the ratio of the change in the ground state energy and change in the entanglement entropy. While the entanglement entropy and the energy diverge, their ratio is a non-divergent quantity. To understand this, let us do a dimensional analysis

$$[E_{D+1}] \propto N^{D+1} \propto \left(\frac{L}{a}\right)^{D+1}, \quad [S_{EE}] \propto \frac{A_D}{a^D} \\ \Rightarrow [\tilde{T}_{EE}] \propto \frac{[E_{D+1}]}{[S_{EE}]} \propto N \frac{L^D}{A_D} \quad (9)$$

$$\text{ie, } \frac{[\tilde{T}_{EE}]}{N} = T_{EE} \propto (N/n)^D \Rightarrow \text{finite} \quad (10)$$

where na is the horizon radius. In the thermodynamic limit, by setting L finite with $N \rightarrow \infty$ and $a \rightarrow 0$, T_{EE} in Eq. (10) is finite.

For large N , we show that, in the natural units, the above calculated temperature is identical to Hawking temperature for the corresponding black-hole [36]:

$$T_{BH} = \frac{\kappa}{2\pi} = \frac{1}{4\pi} \left. \frac{df(\tilde{r})}{d\tilde{r}} \right|_{\tilde{r}=r_h} \quad (11)$$

In the rest of this letter, for different black-hole spacetimes we obtain T_{EE} numerically² and show that they match with Hawking temperature.

Schwarzschild (SBH) black holes

The $D+2$ -dimensional Schwarzschild black hole space-time in dimensionless units \tilde{r} is given by the line element in Eq.(2) with $f(\tilde{r})$ is given by:

$$f(\tilde{r}) = 1 - \frac{1}{\tilde{r}^{D-1}} \quad (12)$$

In Fig.(1), we have plotted total energy (in dimensionless units) and EE versus ϵ for 4 and 6-dimensional Schwarzschild space-time, respectively. Note that for 4-dimensions we have computed von Neumann entropy(

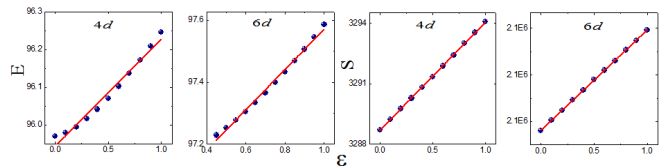


Fig: 1: The total energy (E) of the 4-d and 6-d Schwarzschild black holes are shown respectively in the first and second plots. The third and fourth plots represents its EE as function of ϵ . In this numerical study we set $N = 300$ and $n = 150$. The blue dots are the numerical data and the red straight line is the best fit. In Appendix (A) we have plotted for other values of $n = 50, 80, 100$ and 130.

Rényi entropy for $\alpha = 1$), while for 6-dimensions we have computed for $\alpha > 1$.

We would like to point few things regarding the numerical results: First for every ϵ , Rényi entropy scales approximately as $S_\alpha(r_h/a)^D$. Second, EE and the total energy increases proportional to ϵ . Third, we have plotted the entropy corresponding to the black hole and that scales with ϵ . The entropy corresponding to the scalar field decreases with time (ϵ) as the total system is isolated.

Using the relation (8), we evaluate the temperature numerically. For 4-dimensions, in dimensionless units, we get $T_{EE} = 0.076$ which is close to the value of the Hawking temperature 0.079. In the case of six dimensions, we have evaluated the temperature for different values of α . However, it is important to note that for different values of N , we obtain approximately the same value of entropy. The results are tabulated, see Table(1). For all N , temperature from entanglement entropy $\alpha = 10$ matches with the Hawking temperature.

Reissner-Nordström (R-N) black holes

The four dimensional R-N black hole is given by the line element in Eq.(2), where $f(\tilde{r})$ is

$$f(\tilde{r}) = 1 - \frac{2M/r_h}{\tilde{r}} + \frac{(Q/r_h)^2}{\tilde{r}^2} \quad (13)$$

Q is the charge of the black hole. Note that we have rescaled the radius w.r.t the outer horizon ($r_h = M + \sqrt{M^2 - Q^2}$). Choosing $q = Q/r_h$, we get

$$f(\tilde{r}) = 1 - \frac{(1+q^2)}{\tilde{r}} + \frac{q^2}{\tilde{r}^2} \quad (14)$$

and the black hole temperature in the unit of r_h is $T_{BH} = (1-q^2)/4\pi$. The energy and EE for different q values have the same profile, which looks exactly like in the previous case and is shown in figure(2). As given in the table (1), T_{EE} matches with the Hawking temperature.

² All the computations are done using MATLAB for the lattice size $N = 300$, $10 \leq n \leq 150$ and a minimum accuracy of 10^{-8} . We use central difference scheme i. e. $f'(x) = [f(x+1) - f(x-1)]/(2\Delta x)$.

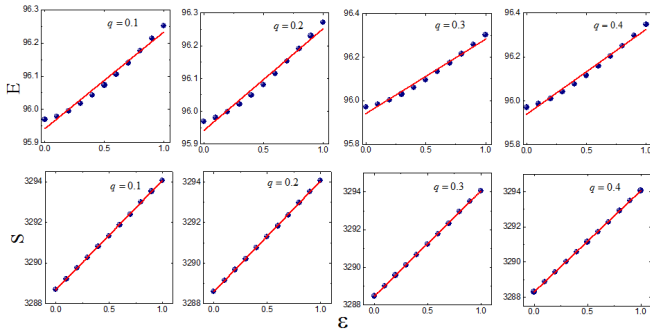


Fig: 2: The first 4 plots in the top panel correspond to total energy (E) and bottom panel is the EE for R-N black hole, as function of ϵ for different q 's. The number of lattice sites used is $N = 300$ and set the horizon at say $n = 150$. The blue dots are the numerical data and the red line is the best linear fit to the data.

Six dimensional Boulware-Deser(B-D) black holes

The six dimensional B-D black hole is given by the line element with $f(\tilde{r})$ [33] is given by

$$f(\tilde{r}) = 1 + \frac{\tilde{r}^2 \tilde{R}_h^2}{6a} \left(1 - \sqrt{1 + \frac{12a}{\tilde{r}^5 \tilde{R}_h^5}} \right) \quad (15)$$

where $a = 12\alpha_{GB} \omega^{-2/3}$, $\tilde{r} = (r\omega^{1/3})/\tilde{R}_h$, and α_{GB} is the Gauss-Bonnet coupling term and \tilde{R}_h is a dimensionless horizon radius and ω , is related to the ADM mass. The black hole temperature in the unit of \tilde{R}_h is [37]

$$T_{BH} = \frac{1}{4\pi} \left(\frac{1 + \tilde{R}_h^3}{2 - \tilde{R}_h^3} \right) \quad (16)$$

For the numerical studies, we set the value of α as 10 and 40 and run the code for the $N = 100$ lattice sites for different α values. The profile of energy and Rényi entropy are same as like in case of lower dimensional black holes. That is, entropy for the scalar field is a decreasing function of ϵ as shown in figure (3).

CONCLUSIONS

In this work, we have shown — for a fixed horizon radius — the ratio of the change in the entanglement entropy at different times and the change the ground state energy at different times is related to the Hawking temperature. It is important to note that entanglement and energy diverges in the limit of $a \rightarrow 0$, however, the *entanglement temperature* is a finite quantity.

Our analysis also shows that the entanglement entropy satisfies all the properties of the black-hole entropy. First, like the black hole entropy, the entanglement entropy increases and never decreases. Second, the entanglement entropy and the temperature satisfies the first law of black-hole mechanics $dE = T_{EE} dS_{EE}$. It is important to

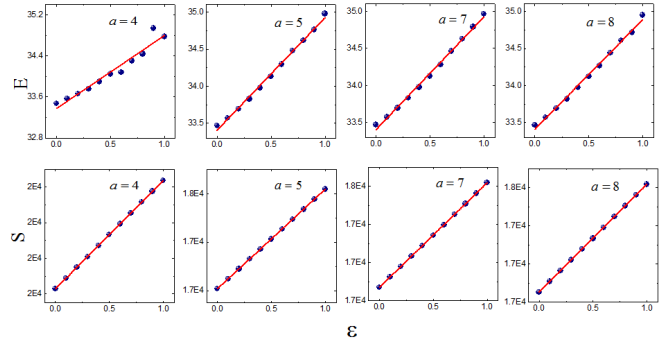


Fig: 3: The first 4 plots in the top panel represents total energy (E) and bottom panel is the Rényi entropy for the B-D black hole, as function of ϵ for different a 's. The number of lattice site used is $N = 100$ and set the horizon at say $n = 50$ and set $\alpha = 10$. The blue dots are the numerical data and the red line is the best linear fit to the data.

Black holes		$\Delta S/\Delta\epsilon$	$\Delta E/\Delta\epsilon$	T_{BH}	T_{EE}
4-d SBH		3.729	0.2846	0.07958	0.07632
R-N	$q = 0.1$	3.747	0.2909	0.07878	0.07764
	$q = 0.2$	3.801	0.3096	0.07639	0.08145
	$q = 0.3$	3.891	0.3414	0.07242	0.08774
	$q = 0.4$	4.011	0.3868	0.06685	0.09643
6-d SBH					
B-D	$\alpha = 10$				
	$a = 4$	320	1.422	0.03985	0.0444
	$a = 5$	373	1.518	0.03982	0.0408
	$a = 7$	479	1.52	0.0398	0.0317
	$a = 8$	552	1.479	0.0398	0.0268
	$\alpha = 40$				
	$a = 4$	227	1.422	0.03985	0.25
	$a = 5$	281	1.518	0.03982	0.216
$a = 7$	453	1.52	0.0398	0.134	
$a = 8$	501	1.479	0.0398	0.118	

Table: 1: The table contains *entanglement temperature* and black hole temperature (measure in units of r_h or \tilde{R}_h) for 4- and 6-dimensional Schwarzschild, 4-dimensional Reissner-Nördstrom, 6-dimensional Boulware-Deser space-times.

note that in higher-dimensions, the temperature is linked to the arbitrary Rényi parameter (α). Recently, Baez has given a physical understanding of the parameter in the canonical ensemble picture [38]. It may be interesting to find such an understanding in the microcanonical ensemble picture.

While the unitary quantum time-evolution is reversible and retains all information about the initial state, we have shown that the restriction of the degrees of freedom outside the event-horizon at all times leads to temperature analogous to Hawking temperature. Our analysis may have relevance to the eigen-state thermalization hypothesis [39–41], which we plan to explore in the future work.

ACKNOWLEDGEMENTS

The work is supported by Max Planck-India Partner Group on Gravity and Cosmology. SSK acknowledges CSIR, Govt. of India, for the financial support. SS is partially supported by Ramanujan Fellowship of DST, India.

* email: santhu@iisertvm.ac.in

† email: shanki@iisertvm.ac.in

- [1] L. D. Landau and E. M. Lifshitz, *Statistical Physics*, vol. V of *Course of Theoretical Physics* (Elsevier, 1980), 3rd ed.
- [2] S. Lloyd, *Nature Physics* **2**, 727 (2006).
- [3] F. G. S. L. Brando and M. B. Plenio, *Nature Physics* **4**, 873 (2008).
- [4] M. Horodecki, *Nature Physics* **4**, 833 (2008).
- [5] S. Popescu and D. Rohrlich, *Phys. Rev. A* **56**, R3319 (1997).
- [6] V. Vedral and M. B. Plenio, *Phys. Rev. A* **57**, 1619 (1998).
- [7] M. B. Plenio and V. Vedral, *Contemporary Physics* **39**, 431 (1998).
- [8] A. Osterloh, L. Amico, G. Falci, and R. Fazio, *Nature* **416**, 608 (2002).
- [9] L.-A. Wu, M. S. Sarandy, and D. A. Lidar, *Phys. Rev. Lett.* **93**, 250404 (2004).
- [10] V. Yukalov, *Laser Physics Letters* **8**, 485 (2011).
- [11] J. Bekenstein, *Lettere Al Nuovo Cimento Series 2* **4**, 737 (1972).
- [12] J. D. Bekenstein, *Phys. Rev. D* **7**, 2333 (1973).
- [13] J. D. Bekenstein, *Phys. Rev. D* **9**, 3292 (1974).
- [14] T. Jacobson, *Phys. Rev. Lett.* **75**, 1260 (1995).
- [15] T. Padmanabhan, *Reports on Progress in Physics* **73**, 046901 (2010).
- [16] E. Verlinde, *Journal of High Energy Physics* **2011** (2011).
- [17] A. Sakharov, *Sov.Phys.Dokl.* **32**, 365 (2000).
- [18] R. Horodecki, P. Horodecki, M. Horodecki, and K. Horodecki, *Rev. Mod. Phys.* **81**, 865 (2009).
- [19] J. Eisert, M. Cramer, and M. B. Plenio, *Rev. Mod. Phys.* **82**, 277 (2010).
- [20] L. Bombelli, R. K. Koul, J. Lee, and R. D. Sorkin, *Phys. Rev. D* **34**, 373 (1986).
- [21] M. Srednicki, *Phys. Rev. Lett.* **71**, 666 (1993).
- [22] M. B. Plenio, J. Eisert, J. Dreißig, and M. Cramer, *Phys. Rev. Lett.* **94**, 060503 (2005).
- [23] S. Das and S. Shankaranarayanan, *Phys. Rev. D* **73**, 121701 (2006).
- [24] S. Das, S. Shankaranarayanan, and S. Sur, *Black hole entropy from entanglement: A review* edited by M. Everett and L. Pedroza, vol. 268 of *Horizons in World Physics* (Nova Science Publishers., New York, 2009), page 211.
- [25] S. N. Solodukhin, *Living Reviews in Relativity* **14** (2011), ISSN 1433-8351.
- [26] S. Braunstein, S. Das, and S. Shankaranarayanan, *Journal of High Energy Physics* **2013**, 130 (2013).
- [27] K. Mallayya, R. Tibrewala, S. Shankaranarayanan, and T. Padmanabhan, *Phys. Rev. D* **90**, 044058 (2014).
- [28] P. Calabrese and J. Cardy, *Journal of Statistical Mechanics: Theory and Experiment* **2004**, P06002 (2004).
- [29] S. Mukohyama, M. Seriu, and H. Kodama, *Phys. Rev. D* **58**, 064001 (1998).
- [30] H. Terashima, *Phys. Rev. D* **61**, 104016 (2000).
- [31] L. D. Landau and E. M. Lifshitz, *The Classical Theory of Fields*, vol. II of *Course of Theoretical Physics* (Butterworth-Heinemann, 1975), 4th ed.
- [32] S. Das, S. Shankaranarayanan, and S. Sur, *Phys. Rev. D* **77**, 064013 (2008).
- [33] D. G. Boulware and S. Deser, *Phys. Rev. Lett.* **55**, 2656 (1985).
- [34] D. J. Toms, *The Schwinger action principle and effective action*, Cambridge monographs on mathematical physics (Cambridge Univ. Press, Cambridge, 2007).
- [35] H. Sakaguchi, *Progress of Theoretical Physics* **81**, 732 (1989).
- [36] S. W. Hawking, *Communications in Mathematical Physics* **43**, 199 (1975).
- [37] R. C. Myers and J. Z. Simon, *Phys. Rev. D* **38**, 2434 (1988).
- [38] J. C. Baez, arXiv:1102.2098 [quant-ph] (2011).
- [39] M. Srednicki, *Phys. Rev. E* **50**, 888 (1994).
- [40] M. Rigol and M. Srednicki, *Phys. Rev. Lett.* **108**, 110601 (2012).
- [41] R. Nandkishore and D. A. Huse, *Annual Review of Condensed Matter Physics* **6**, 15 (2015).

Appendix-A : Calculation of Scalar field Hamiltonian in Lemaitre coordinate

In this appendix, we give details of the derivation of the Hamiltonian in Eq:(6) upto second order in ϵ . The canonical action after the infinitesimal transformation in eq:(5) is,

$$\begin{aligned}
 S \simeq & \frac{1}{2} \sum_{l, m_i} \int d\tilde{\tau} d\tilde{\xi} (\tilde{r} + \epsilon h_1 + \epsilon^2 h_2/2)^D \left[\left(1 - f - \epsilon h_1 \frac{\partial f}{\partial \tilde{r}} - \frac{\epsilon^2}{2} \left[h_2 \frac{\partial f}{\partial \tilde{r}} + h_1^2 \frac{\partial^2 f}{\partial \tilde{r}^2} \right] \right)^{1/2} (\partial_{\tilde{\tau}} \tilde{\Phi}_{lm_i})^2 \right. \\
 & - \left. \left(1 - f - \epsilon h_1 \frac{\partial f}{\partial \tilde{r}} - \frac{\epsilon^2}{2} \left[h_2 \frac{\partial f}{\partial \tilde{r}} + h_1^2 \frac{\partial^2 f}{\partial \tilde{r}^2} \right] \right)^{-1/2} (\partial_{\tilde{\xi}} \tilde{\Phi}_{lm_i})^2 - \frac{l(l+D-1)}{(\tilde{r} + \epsilon h_1 + \epsilon^2 h_2/2)^2} \right. \\
 & \left. \times \left(1 - f - \epsilon h_1 \frac{\partial f}{\partial \tilde{r}} - \frac{\epsilon^2}{2} \left[h_2 \frac{\partial f}{\partial \tilde{r}} + h_1^2 \frac{\partial^2 f}{\partial \tilde{r}^2} \right] \right)^{1/2} \tilde{\Phi}_{lm_i}^2 \right] \quad (17)
 \end{aligned}$$

where $h_1 = \frac{\partial \tilde{r}}{\partial \tau}$, $h_2 = \frac{\partial^2 \tilde{r}}{\partial \tau^2}$. Using the following relation between the Lemaître coordinates

$$\xi - \tau = \int \frac{dr}{\sqrt{1 - f[r(\tau, \xi)]}} \quad (18)$$

we get,

$$h_1 = -\sqrt{1-f}, \quad h_2 = \frac{-1}{2} \frac{\partial f}{\partial \tilde{r}}, \quad \frac{d\tilde{\xi}}{d\tilde{r}}|_{\text{con.}\tilde{\tau}} = \frac{1}{\sqrt{1-f}} \quad (19)$$

The Hamiltonian (H) corresponding to the above Lagrangian is

$$H \simeq \frac{1}{2} \sum_{l, m_i} \int d\tilde{\xi} \left[\tilde{\Pi}_{lm_i}^2 + \frac{g_1^D}{g_2} \left(\partial_{\tilde{\xi}} \frac{\tilde{\chi}_{lm_i}}{g_1^{D/2} \sqrt{g_2}} \right)^2 + \frac{l(l+D-1)}{g_1^2} \tilde{\chi}_{lm_i}^2 \right] \quad (20)$$

where

$$g_1 = \tilde{r} + \epsilon h_1 + \epsilon^2 h_2 / 2, \quad g_2 = \sqrt{1 - f - \epsilon h_1 \frac{\partial f}{\partial \tilde{r}} - \frac{\epsilon^2}{2} \left[h_2 \frac{\partial f}{\partial \tilde{r}} + h_1^2 \frac{\partial^2 f}{\partial \tilde{r}^2} \right]}, \quad \tilde{\chi}_{lm_i} = g_1^{D/2} \sqrt{g_2} \tilde{\Phi}_{lm_i} \quad (21)$$

and $\tilde{\Pi}_{lm_i}$ is the canonical conjugate momenta corresponding to the field $\tilde{\chi}_{lm_i}$.

Upon quantization, $\tilde{\Pi}_{lm_i}$ and $\tilde{\chi}_{lm_i}$ satisfy the usual canonical commutation relation:

$$\left[\tilde{\chi}_{lm_i}(\tilde{\xi}, \tilde{\tau}), \tilde{\Pi}_{l'm'_i}(\tilde{\xi}', \tilde{\tau}) \right] = i \delta_{ll'} \delta_{m_i m'_i} \delta(\tilde{\xi} - \tilde{\xi}') \quad (22)$$

Using relations (19) and expanding the Hamiltonian up to second order in ϵ , we get,

$$H \simeq \frac{1}{2} \sum_{l, m_i} \int_{\tilde{\tau}}^{\infty} d\tilde{r} \left[\pi_{lm_i}^2 + \tilde{r}^D \frac{(1 - \epsilon H_1 - \epsilon^2 H_2)^D}{(1 + \epsilon H_3 - \epsilon^2 H_4)^{1/2}} \left[\partial_{\tilde{r}} \frac{\sigma_{lm_i}}{\tilde{r}^{D/2} (1 - \epsilon H_1 - \epsilon^2 H_2)^{D/2} (1 + \epsilon H_3 - \epsilon^2 H_4)^{1/4}} \right]^2 + \frac{l(l+D-1)}{\tilde{r}^2 (1 - \epsilon H_1 - \epsilon^2 H_2)^2} \sigma_{lm_i}^2 \right] \quad (23)$$

The Hamiltonian in Eq. (23) is of the form $H \simeq H_0 + \epsilon V_1 + \epsilon^2 V_2$, where H_0 is the unperturbed scalar field Hamiltonian in the flat space-time, V_1 and V_2 are the perturbed parts of the Hamiltonian given by;

$$H_0 = \frac{1}{2} \sum_{l, m_i} \int_{\tilde{\tau}}^{\infty} d\tilde{r} \left[\pi_{lm_i}^2 + \tilde{r}^D \left[\partial_{\tilde{r}} \frac{\sigma_{lm_i}}{\tilde{r}^{D/2}} \right]^2 + \frac{l(l+D-1)}{\tilde{r}^2} \sigma_{lm_i}^2 \right] \quad (24a)$$

$$V_1 = \frac{1}{2} \sum_{l, m_i} \int_{\tilde{\tau}}^{\infty} d\tilde{r} \left[\frac{(-D \sigma_{lm_i} + 2\tilde{r} \sigma'_{lm_i}) (DH_3 \sigma_{lm_i} - 2\tilde{r} H_3 \sigma'_{lm_i} + 2D\tilde{r} H_1' \sigma_{lm_i} - \tilde{r} H_3' \sigma_{lm_i})}{4\tilde{r}^2} + \frac{2l(l+D-1)H_1}{\tilde{r}^2} \sigma_{lm_i}^2 \right] \quad (24b)$$

$$V_2 = \frac{1}{2} \sum_{l, m_i} \int_{\tilde{\tau}}^{\infty} d\tilde{r} \left[(H_3^2 + H_4) \sigma_{lm_i}^2 + \left(-\frac{DH_3^2}{\tilde{r}} - \frac{DH_4}{\tilde{r}} + DH_1 H_1' - DH_3 H_1' + DH_2' + H_3 H_3' + \frac{1}{2} H_4' \right) \sigma'_{lm_i} \sigma_{lm_i} + \left(\frac{l(l+D-1)(3H_1^2 + 2H_2)}{\tilde{r}^2} + \frac{D^2 H_3^2}{4\tilde{r}^2} + \frac{D^2 H_4}{4\tilde{r}^2} - \frac{D^2 H_1 H_1'}{2\tilde{r}} + \frac{D^2 H_3 H_1'}{2\tilde{r}} + \frac{1}{4} D^2 H_1'^2 - \frac{D^2 H_2'}{2\tilde{r}} - \frac{DH_3 H_3'}{2\tilde{r}} - \frac{1}{4} DH_1' H_3' + \frac{1}{16} H_3'^2 - \frac{dH_4'}{4\tilde{r}} \right) \sigma_{lm_i}^2 \right] \quad (24c)$$

where

$$H_1 = \frac{\sqrt{1-f}}{\tilde{r}}, \quad H_2 = \frac{1}{4\tilde{r}} \frac{\partial f}{\partial \tilde{r}}, \quad H_3 = \frac{1}{\sqrt{1-f}} \frac{\partial f}{\partial \tilde{r}}, \quad H_4 = \frac{-1}{4(1-f)} \left(\frac{\partial f}{\partial \tilde{r}} \right)^2 + \frac{1}{2} \frac{\partial^2 f}{\partial \tilde{r}^2} \quad (25)$$

and the redefined field operators are

$$\tilde{\Pi}_{lm_i} = \frac{\pi_{lm_i}}{(1-f)^{1/4}} \quad \text{and} \quad \tilde{\chi}_{lm_i} = \frac{\sigma_{lm_i}}{(1-f)^{1/4}} \quad (26)$$

such that they satisfy the following canonical commutation relation

$$[\pi_{lm_i}(\tilde{r}, \tilde{\tau}), \sigma_{l'm'_i}(\tilde{r}', \tilde{\tau})] = i\delta_{ll'}\delta_{m_im'_i}\delta(\tilde{r} - \tilde{r}') \quad (27)$$

Appendix-B : Plots of internal energy as well as EE as a function of ϵ for different black hole space-time

In this Appendix, we give plots of EE for different space-times;

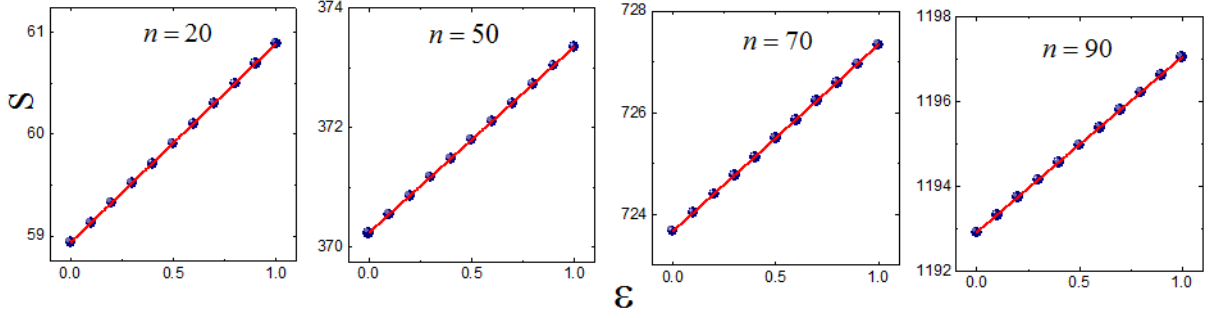


Fig: 4: Plots of the EE as function of ϵ for the 4-d Schwarzschild black hole with $N = 200$, $n = 20, 50, 70$, and 90 , respectively. The blue dots are the numerical data and the red line is the best linear fit to the data.

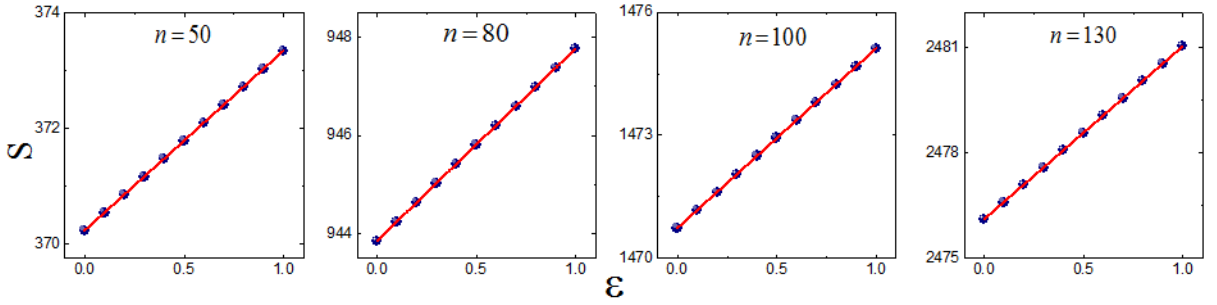


Fig: 5: Plots of the EE as function of ϵ for the 4-d Schwarzschild black hole with $N = 300$, $n = 50, 80, 100$, and 130 , respectively. The blue dots are the numerical data and the red line is the best linear fit to the data.

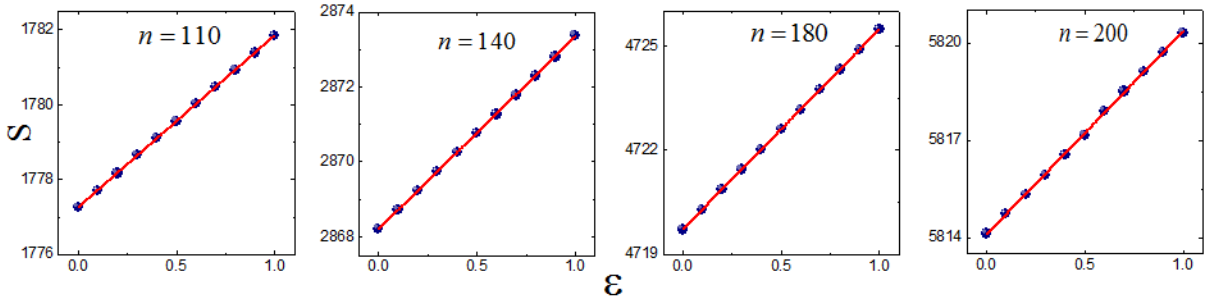


Fig: 6: Plots of the EE as function of ϵ for the 4-d Schwarzschild black hole with $N = 400$, $n = 110, 140, 180$, and 200 respectively. The blue dots are the numerical data and the red line is the best linear fit to the data.

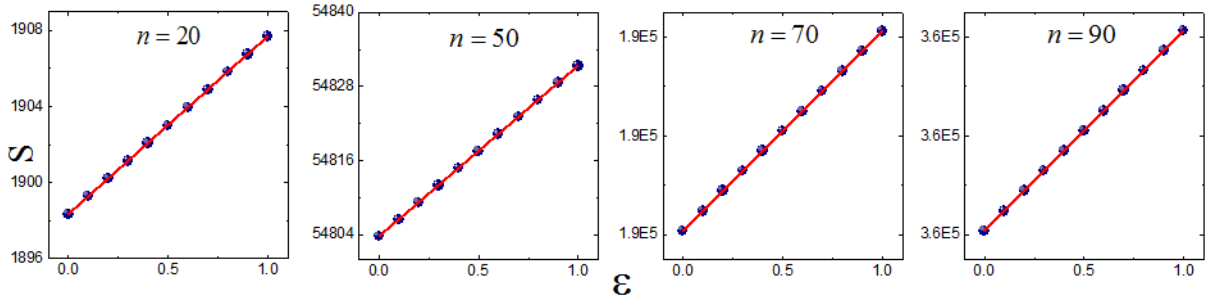


Fig. 7: Plots of the EE as function of ϵ for the 6-d Schwarzschild black hole with $N = 200$, $\alpha = 10$ and $n = 20, 50, 70$, and 90 , respectively. The blue dots are the numerical data and the red line is the best linear fit to the data.

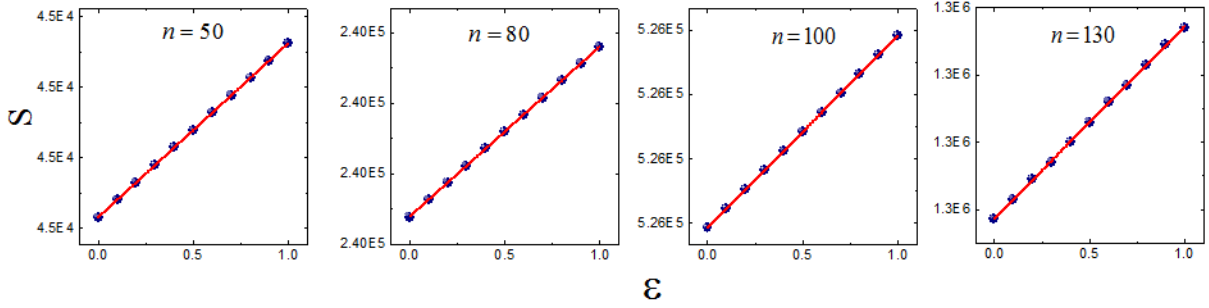


Fig. 8: Plots of the EE as function of ϵ for the 6-d Schwarzschild black hole with $N = 300$, $\alpha = 10$ and $n = 50, 80, 100$, and 130 , respectively. The blue dots are the numerical data and the red line is the best linear fit to the data.

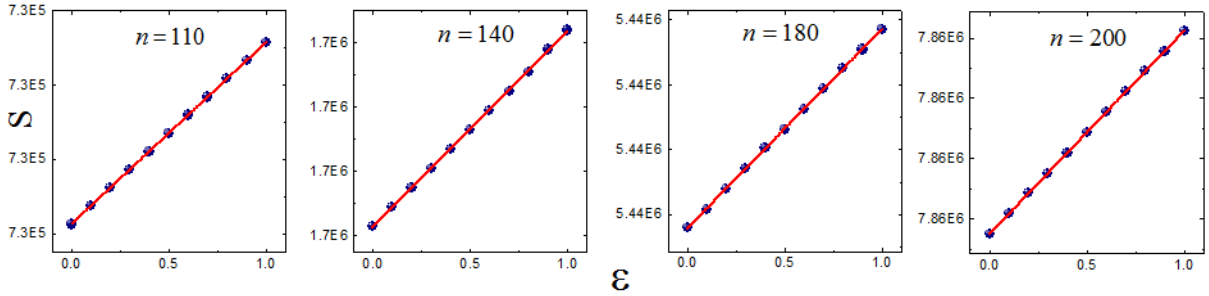


Fig. 9: Plots of the EE as function of ϵ for the 6-d Schwarzschild black hole with $N = 400$ and $\alpha = 10$ and $n = 110, 140, 180$, and 200 , respectively. The blue dots are the numerical data and the red line is the best linear fit to the data.

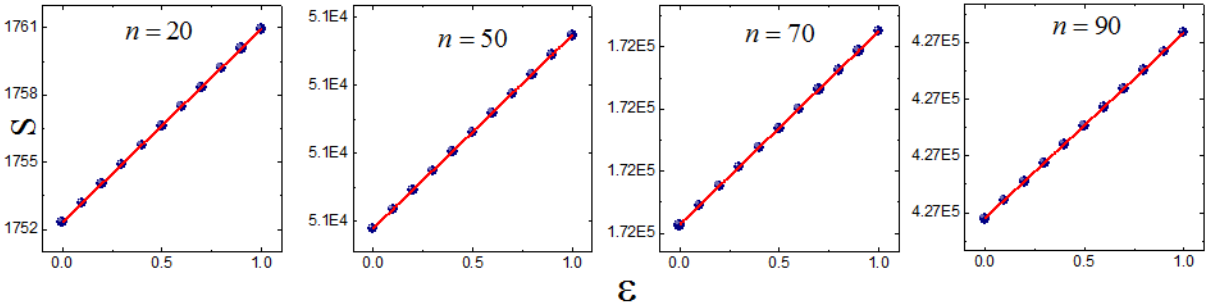


Fig. 10: Plots of the EE as function of ϵ for the 6-d Schwarzschild black hole respectively. The number of lattice sites used is $N = 200$, $\alpha = 40$ and $n = 20, 50, 70$, and 90 , respectively. The blue dots are the numerical data and the red line is the best linear fit to the data.

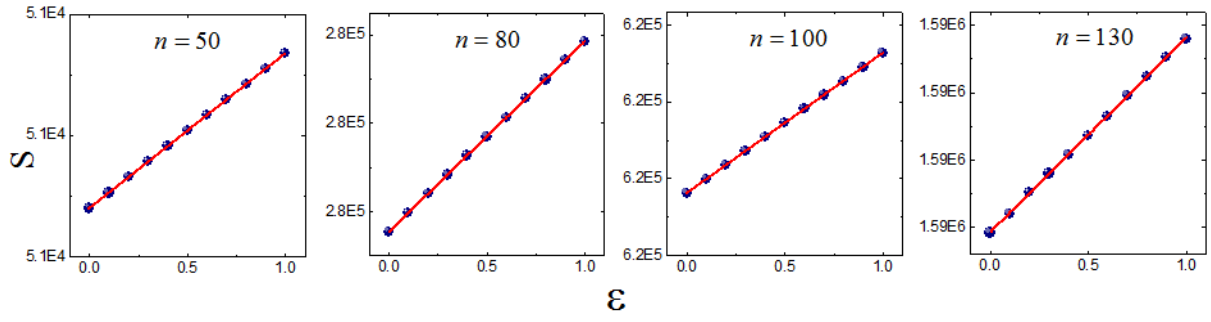


Fig: 11: Plots of the EE as function of ϵ for the 6-d Schwarzschild black hole with $N = 300, \alpha = 40$ and $n = 50, 80, 100,$ and $130,$ respectively. The blue dots are the numerical data and the red line is the best linear fit to the data.

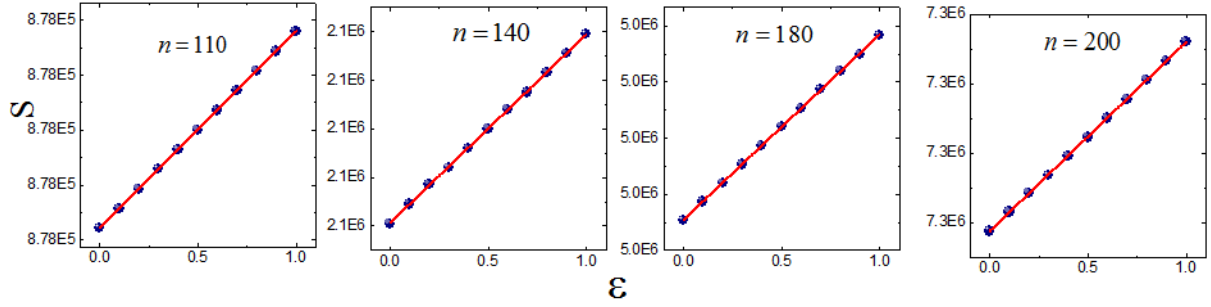


Fig: 12: Plots of the EE as function of ϵ for the 6-d Schwarzschild black hole with $N = 400, \alpha = 40$ and $n = 110, 140, 180,$ and $200,$ respectively. The blue dots are the numerical data and the red line is the best linear fit to the data.

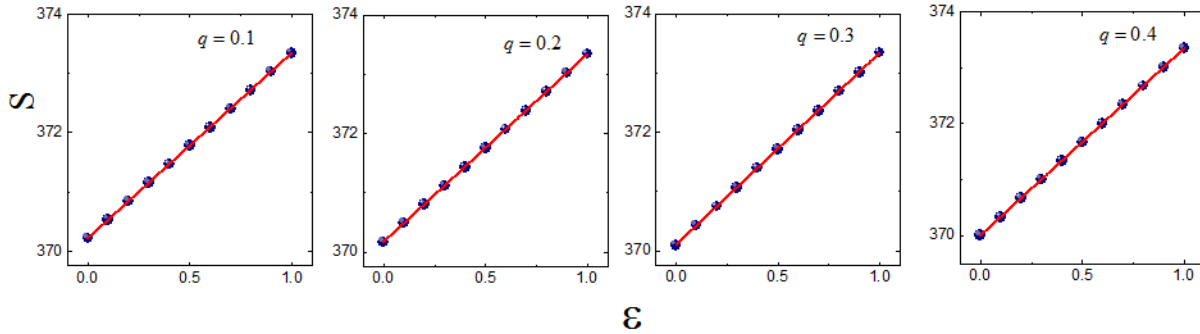


Fig: 13: Plots of the EE of R-N black hole in terms of ϵ for different q 's with $N = 300,$ and $n = 50.$ The blue dots are the numerical data and the red line is the best linear fit to the data.

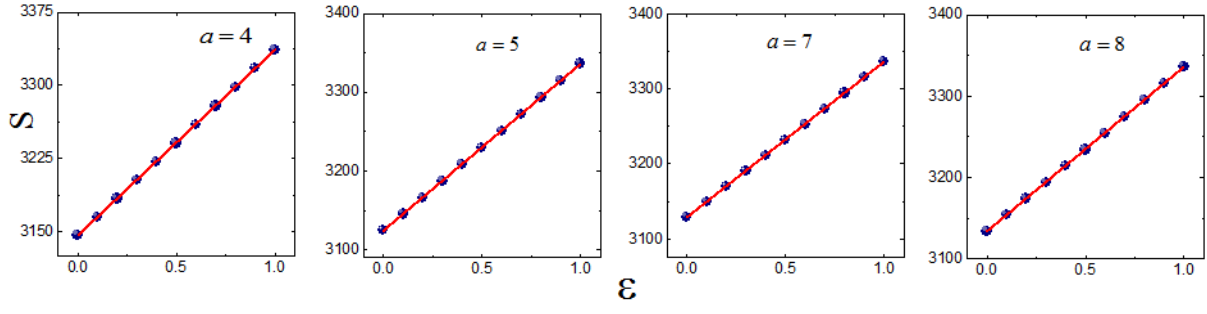


Fig: 14: Plots of the Rényi entropy of the B-D black hole with different a 's with $N = 100$, $n = 30$, and $\alpha = 10$. The blue dots are the numerical data and the red line is the best linear fit to the data.

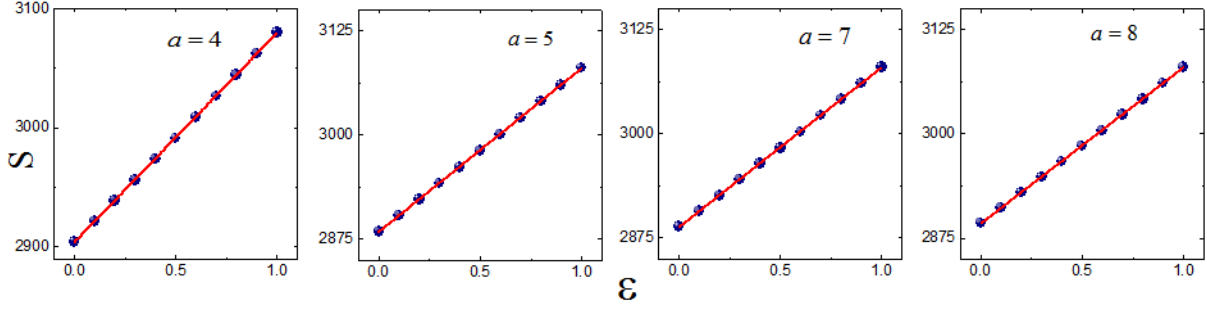


Fig: 15: Plots of Rényi entropy of the B-D black hole with different a 's with $N = 100$, $n = 30$, and $\alpha = 40$. The blue dots are the numerical data and the red line is the best linear fit to the data.